Chemical Science

Cite this: *Chem. Sci.*, 2012, **3**, 433

www.rsc.org/chemicalscience

EDGE ARTICLE

Synthesizing MnO_2 nanosheets from graphene oxide templates for high performance pseudosupercapacitors†

Guixia Zhao,[a] Jiaxing Li,[a] Lang Jiang,[b] Huanli Dong,[b] Xiangke Wang*[a] and Wenping Hu*[b]

Received 26th September 2011, Accepted 13th October 2011
DOI: 10.1039/c1sc00722j

A facile method to synthesize layered manganese oxide nanosheets was developed for the first time by using graphene oxide as a template. The *in situ* replacement of carbon atoms on the graphene oxide framework by edge-shared [MnO_6] octahedra provides a new methodology to synthesize graphene-based two-dimensional nanomaterials. The transformation of graphene oxide into δ-type MnO_2 nanosheets results in an especially high surface area (157 $m^2\ g^{-1}$), which is the highest value amongst today's MnO_2 nanomaterials. Moreover, the MnO_2 nanosheets demonstrated prominent capacitance (~1017 F g^{-1} at a scan rate of 3 mV s^{-1}, and ~1183 F g^{-1} at a current density of 5 A g^{-1}) and remarkable rate capability (~244 F g^{-1} at a high scan rate of 50 mV s^{-1} and ~559 F g^{-1} at a high current density of 25 A g^{-1}), indicating their promise in high energy and power density pseudosupercapacitors.

Introduction

Supercapacitors are the current ideal candidates for green energy storage under the energy-shortage condition and given the urgent pollution issue situation.[1–4] Among the two major categories of supercapacitors, *i.e.*, electric double layer supercapacitors and Faraday pseudocapacitance supercapacitors, Faraday pseudocapacitance is 10–100 times higher than electric double layer capacitance, due to a fast and highly reversible redox reaction.[5,6] According to previous research,[7,8] the reversibility of the redox reaction, and the morphology and structure of the active materials are crucial to the performance of a Faraday pseudosupercapacitor. Therefore, the search for a highly reversible redox reaction and special nanomaterials with large specific surface areas and intriguing morphologies favorable for the redox reaction is the most pressing challenge. Although Wang *et al.*[9] reported advanced electrochemical pseudocapacitor $Ni(OH)_2$ nanoplates, with a high specific capacitance of ~1335 F g^{-1} at a charge and discharge current density of 2.8 A g^{-1}, the specific capacitance of most supercapacitor materials reported has been less than 1000 F g^{-1}.[10–13]

As a cheap and frequently-used electrochemical capacitor material,[14–17] manganese oxide produced by traditional or improved methods[18–22] has a low specific surface area and shows poor performance. Herein, we introduce a facile approach to synthesize layered MnO_2 nanosheets with high specific surface area and prominent specific capacitance which works effectively as a pseudosupercapacitor material for energy storage. Herein, graphene oxide was selected as a template because (i) it is expected that carbon atoms in the graphene framework would reduce MnO_4^- ions *in situ* to form Mn(IV); (ii) the high hydrophilicity of graphene oxide makes MnO_4^- ions react with every graphite layer, leading to the simultaneous complete replacement of the template by the MnO_2 nanosheets; (iii) the oxidation of graphene oxide by $KMnO_4$ proceeds in aqueous solution under mild conditions (see details in the experimental section in the ESI†). Therefore, the synthesis of layered MnO_2 nanosheets is largely facilitated compared with the exfoliation of various types of layered manganese oxide using large molecules of the past decades,[23–29] which were complicated and under harsh conditions.

Results and discussion

Materials characterization

Fig. 1a–c depicts different magnifications and HRTEM images of as-prepared MnO_2, which reveals abundant two-dimensional (2D) nanosheets. The lateral view shows the layered-structure of the nanosheets, and the HRTEM image gives a 0.71 nm basal spacing. The selected area electron diffraction (SAED) pattern detected in the normal direction of the nanosheets reveals only a weak reflection halo (indexed to 0.71 nm *d*-spacing), which is indexed to δ-MnO_2 projected along the [001] zone axis. Such an

[a]*Key Laboratory of Novel Thin Film Solar Cells, Institute of Plasma Physics, Hefei, 230031, P. R. China. E-mail: xkwang@ipp.ac.cn; Fax: +86-551-5591310; Tel: +86-551-5592788*
[b]*Beijing National Laboratory for Molecular Sciences, Key Laboratory of Organic Solids, Institute of Chemistry, Chinese Academy of Sciences, Beijing, 100190, P. R. China. E-mail: huwp@iccas.ac.cn; Fax: +86-10-62527295; Tel: +86-10-82615030*

† Electronic supplementary information (ESI) available: Synthesis of the material and characterization method, FT-IR spectrum and TGA of MnO_2 nanosheets, electrochemical measurement, the specific capacitance calculation and blank control experimental results by the electrochemical measurements. See DOI: 10.1039/c1sc00722j

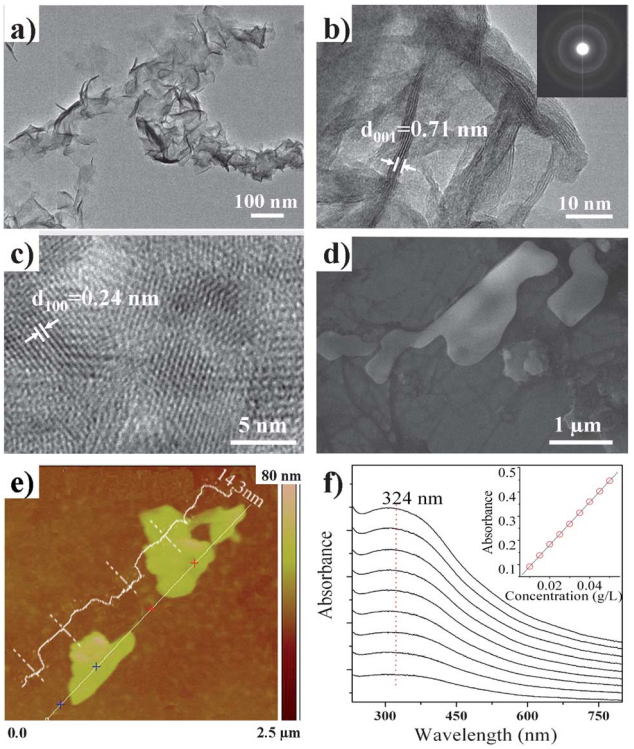

Fig. 1 (a–c) TEM images of MnO_2 nanosheets and corresponding SAED pattern; (d) SEM image of MnO_2 nanosheets on a mica substrate; (e) AFM image of MnO_2 nanosheets on a mica substrate. (f) UV-Vis absorption spectra of MnO_2 nanosheets at different concentrations, and the absorbance at 324 nm plotted against the concentration of MnO_2 nanosheets (inset figure).

SAED pattern supports the lamellar structure of the nanosheets. HRTEM also indicates a 0.24 nm lattice spacing of the (100) planes of MnO_2.[30] An energy dispersive spectrum (EDS) taken from the nanosheets confirms the absence of graphene oxide and the existence of MnO_2 nanosheets (Fig. S1†). The SEM image (Fig.1d) shows the lateral size is several hundred nanometres, even to 1∼2 μm. From the AFM image (Fig. 1e), the thickness and lateral size of the MnO_2 nanosheets are quite in accordance with the TEM and SEM analyses. The morphology characterization indicates that the synthesized MnO_2 are layer-structured nanosheets with an average width to thickness ratio of ∼100. According to our previous research on graphene,[31] the lateral size of the synthesized MnO_2 nanosheets is comparable to that of graphene nanosheets, which is in good agreement with the inferred *in situ* replacement mechanism. The nanostructure of the layered MnO_2 nanosheets is further confirmed by UV-Vis adsorption spectra (Fig. 1f). The MnO_2 nanosheets show a broad absorption peak from 200 nm to 400 nm, which is a typical optical characteristic of the nanomaterials according to previous investigation.[23] The molar extinction coefficient (ε) at the peak maxima (324 nm) is 7.72×10^2 mol^{-1} dm^3 cm^{-1}.

As shown in Fig. 2a, the basal diffraction peaks of the layered hexagonal system, indexed as (001), are not revealed as spikes, except for the tiny peak at $2\theta = 12.1°$, which corresponds to the diffraction of (001) resulting from the weak intrasheet diffraction ($d_{001} = 0.73$ nm). The interlayer spacing is consistent with that analyzed by TEM. The small peaks at $2\theta = 36°$ and 65° are

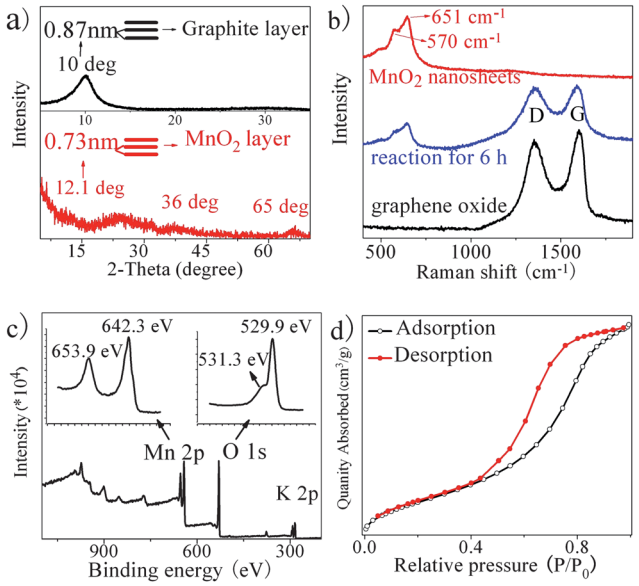

Fig. 2 (a) XRD patterns of layered graphene oxide sheets (upper line) and MnO_2 nanosheets (lower line); (b) Raman spectra of layered graphene oxide, the sample after a reaction time of 6 h and the final synthesized MnO_2 nanosheets; (c) XPS spectrum of MnO_2 nanosheets (642.3eV and 653.9 eV correspond to Mn $2p_{3/2}$ and Mn $2p_{1/2}$; 529.9 eV and 531.3 eV correspond to O 1s in the lattice of [MnO_6] octahedra and in the interlayer H_2O); (d) N_2 adsorption–desorption isotherms of the MnO_2 nanosheets at a degas temperature of 300 °C.

indexable as (100) and (110) for a hexagonal 2D unit cell with $a =$ 0.30 nm. What is more, the wide and broad diffraction pattern between 15° and 35° has been demonstrated in detail in previous reports,[23,25,26,32–34] and this broad profile can be understood in terms of scattering from an individual MnO_2 layer and is evidence of the formation of the layered MnO_2 nanosheets. The contrast of the graphene oxide sheets and the as-prepared MnO_2 nanosheets is inset in the XRD patterns. In order to investigate the *in situ* transformation process of graphene oxide to MnO_2 nanosheets, samples were taken from the reaction mixtures after a reaction time of 6 h, and characterized by Raman spectroscopy (Fig. 2b). The decrease of the D and G bands in the graphitic 2D hexagonal lattice and the appearance of the peaks located at 570 and 651 cm^{-1}, which are due to the Mn–O lattice vibrations,[32–36] also confirm the yield of MnO_2 and the depletion of graphene oxide. The complete disappearance of the D and G bands in the final sample suggests the transformation of graphene oxide to MnO_2 nanosheets, instead of graphene oxide–MnO_2 composites. According to the X-ray photoelectron spectroscopy (XPS) analysis (Fig. 2c), the peaks of Mn $2p_{3/2}$ at 642.3 eV and $2p_{1/2}$ at 653.9 eV, with a spin-energy separation of 11.6 eV, demonstrate the existence of MnO_2.[37,38] It is necessary to note that the peak of O 1s includes a spiking at 529.9 eV and a relatively weak peak at 531.3 eV, which correspond to two kinds of oxygen: one in the lattice of [MnO_6] octahedra, and the other in the interlayer H_2O.[39,40] The atomic ratio of K/Mn is about 0.17. Thereby, the MnO_2 nanosheets can be written as $K_{0.17}MnO_2$, with a small quantity of K^+ ions in the interlayer to balance the negative charge of the MnO_2 layer. The atomic ratio in the MnO_2 nanosheets is in good agreement with that found by EDS analysis (Fig. S1†).

The N_2-BET surface area of the MnO_2 nanosheets exhibits as high as 157 $m^2\ g^{-1}$ (the N_2 adsorption–desorption isotherms are shown in Fig. 2d), with the t-plot external surface area up to 135 $m^2\ g^{-1}$, which is much higher than that of MnO_2 synthesized by other methods.[41,42] The large external surface area is coincident with the lamellar morphology of MnO_2. The FT-IR spectrum shows the characteristic absorbances of the Mn–O stretching vibration at 530, 473 and 411 cm^{-1},[43] and the interlayer water absorption bands at 3414 and 1630 cm^{-1} (Fig. S2†).[25] The existence of interlayer water corresponds to the layered structure of MnO_2. The small absorption bands at 1530 and 1450 cm^{-1} are due to the small quantity of residual carbonate in the MnO_2 nanosheets.[44] In the thermogravimetric analysis (TGA) (Fig. S3†), the DTA curve shows endothermic peaks at 103.5 °C, which correspond to the evaporation of surface absorbed water. The TG curve indicates that the weight loss of surface absorbed water is about 5.1% and a further weight loss (11.6%) observed from 126 °C to 400 °C is attributed to the dehydration of interlayer water.[45] The exothermic peak around 549.2 °C is due to the transformation of MnO_2 into Mn_2O_3 by the evolution of oxygen.[25,45] The TGA confirms the layered structure and also demonstrates the species of the as-prepared manganese oxide. All of these characterizations are in good conformity with each other, which strongly indicates the successful transformation of layered graphene oxide into MnO_2 nanosheets.

Proposed mechanism of the synthesis

The whole mechanism of the layered MnO_2 nanosheet formation is illustrated in Fig. 3. From the characterization, the final materials are layered MnO_2 nanosheets without any graphene oxide. Considering the completely redox reaction between graphene oxide and MnO_4^-, and the incomplete oxidation of graphene by MnO_4^- as reported by Chen *et al.*,[42] who fabricated MnO_2 with a specific surface area of 50.3 $m^2\ g^{-1}$ using graphene exfoliated from graphite by *N*-methyl-pyrrolidone, we herein infer that the redox reaction involves every graphene oxide layer. The highly hydrophilic graphene oxide sheets ensure that the MnO_4^- ions react with every graphene oxide layer, while the graphene exfoliated from graphite by *N*-methyl-pyrrolidone does not possess this superiority. What is more, the layered structure of the synthesized MnO_2 nanosheets, which seems to be a duplicate of the graphene morphology, is considered to be more an outcome of the replacement of the carbon atoms by [MnO_6] octahedra than that of the formation of MnO_2 layers between the graphene oxide layers. In the undisturbed reaction system, the C–C bonds were then broken and the carbon atoms were fully oxidized to form CO_2 or CO_3^{2-}. Simultaneously, the MnO_4^- was reduced to form [MnO_6] octahedra, and the neighboring [MnO_6] octahedra edge-shared for energy stabilization.[28] To some extent, the thickness of the as-prepared MnO_2 nanosheets is related to the different layers of the graphene oxides. Therefore, in brief, the layered MnO_2 nanosheets result from the framework substitution of graphene oxide by edge-shared [MnO_6] octahedra through a redox reaction.

Compared with the earlier exfoliation of MnO_2 nanosheets from layered δ-MnO_2, the framework substitution of graphene oxide using $KMnO_4$ as oxidant is more expedient and efficient for the realization of MnO_2 nanosheets of high quality and in large quantities.

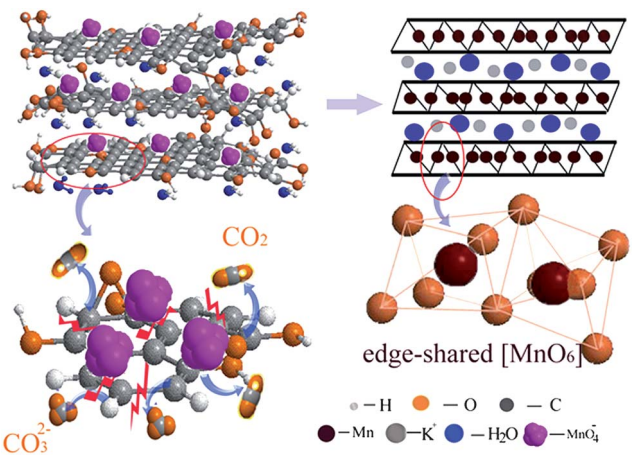

Fig. 3 Illustration of the *in situ* transformation process. The upper pictures represent the transmission from graphene oxide nanosheets to MnO_2 nanosheets, and the lower pictures are magnifications.

Application as pseudocapacitor materials

To investigate their potential application as supercapacitor materials, the MnO_2 nanosheets were used as the active material in a working electrode. Fig. 4a illustrates the cyclic voltammetry (CV) curves of the MnO_2 nanosheets at various scan rates. The symmetrical oxidation peak and reduction peak indicated the

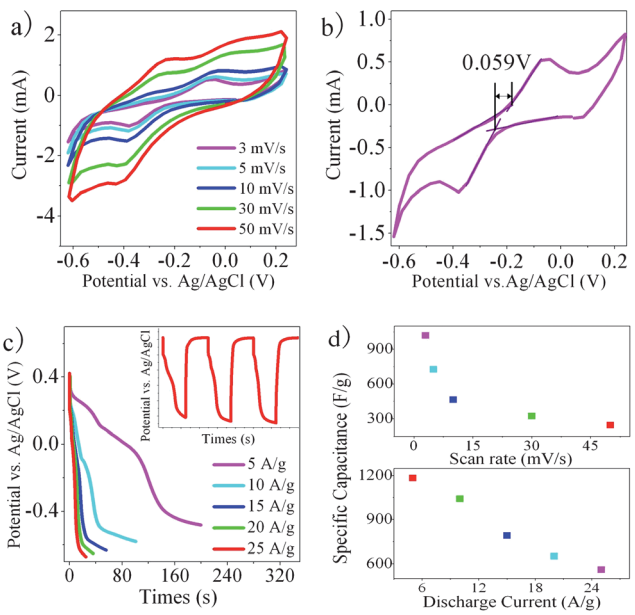

Fig. 4 Electrochemical measurements of MnO_2 nanosheets. (a) CV curves of MnO_2 nanosheets at various scan rates; (b) CV curves of MnO_2 nanosheets at a scan rate of 3 mV s^{-1}, $\Delta E_p = \varphi_{pa} - \varphi_{pc} \approx 0.059$ V; (c) galvanostatic discharge curves of MnO_2 nanosheets at various discharge/charge current densities, the inset figure shows the galvanostatic discharge and charge curves at a current density of 25 A g^{-1}; (d) the calculated specific capacitance of MnO_2 nanosheets corresponding to the CV curves in (a) and the galvanostatic discharge curves in (c).

existence of a highly reversible redox reaction, which is considered to be $MnO_2 + H^+ + e^- \rightleftarrows MnOOH$ or $MnO_2 + K^+ + e^- \rightleftarrows MnOOK$.[7] Considering the low concentration of H^+, the high concentration of K^+ in K_2SO_4 electrolyte and the considerable K^+ in the interlayers of the MnO_2 nanosheets, the latter reaction dominates the redox process. At a low scan rate of 3 mV s^{-1} in the CV curve (Fig.4b), the ΔE_p value of 0.059 V, which is the theoretical potential difference between oxidation and reduction peaks in the completely reversible redox reaction,[46,47] also demonstrates the reversible redox reaction.

The specific capacitance of the MnO_2 nanosheets is calculated to be as high as ~1017 F g^{-1} at a scan rate of 3 mV s^{-1}. Although the specific capacitances at different scan rates show some decrease with the increasing scan rates, the specific capacitance is still high: up to ~244 F g^{-1} at a high scan rate of 50 mV s^{-1} (Fig. 4d). As shown in Fig. 4c and d, the galvanostatic discharge curve at a high discharge/charge current density of 25 A g^{-1} further demonstrates the high performance of the MnO_2 nanosheets as an electrochemical pseudocapacitor material, with a calculated specific capacitance of ~559 F g^{-1}. At a low discharge/charge current density of 5 A g^{-1}, the MnO_2 nanosheets show a specific capacitance as high as ~1183 F g^{-1}. What is most exciting is that the potential is almost unchanged in the charge curves during the discharge/charge cycle (inset in Fig. 4c), reflecting the excellent storage capability, which is probably resulted from the efficient electron transfer in the rapid and reversible redox reaction.

The excellent electrochemical performance of the MnO_2 nanosheets is considered to be due to the special structure and morphology transmitted from the graphene oxide templates. It is understandable that in the MnO_2 nanosheets, the MnO_2 layers and the interlayer K^+ ions take part in the reversible redox reaction *in situ* without the diffusion of K^+ from the electrolyte to the interlayer. What is more important is that the large specific surface area of the MnO_2 nanosheets (157 m^2 g^{-1}) makes the MnO_2 nanosheets disperse quite well in the Ni foam matrix, ensuring the facile diffusion of the K^+ ions from the electrolyte to the surfaces of the MnO_2 layers, which is the main restraining factor for the performance of pseudosupercapacitor materials. Furthermore, the electron transport between the conductive matrix (Ni foam) and the MnO_2 nanosheets is also immensely improved due to the highly homogeneous distribution of the MnO_2 nanosheets. Therefore, the fast and highly reversible redox reaction between Mn(IV) and Mn(III) proceeds reasonably in the neutral electrolyte, giving birth to the excellent storage capability.

Conclusion

In summary, layered MnO_2 nanosheets were synthesized by a facile redox method using layered graphene oxide sheets as templates. The synthesized layered MnO_2 nanosheets completely took the place of the graphene oxide framework and retained the intriguing two-dimensional structure of graphene. The special morphology of the graphene oxide-derived manganese oxide nanosheets ensures the excellent high Faraday pseudocapacitance even at high energy and power densities. Considering the facile synthesis and the prominent electronic properties, the layered MnO_2 nanosheets could become promising supercapacitor materials in future industry.

More importantly, the intriguing structure is believed to largely improve its other applications as a catalyst, adsorbent and degradant *etc*. What is more encouraging is that the utilization of graphene oxide as a template opens a new application for its special two-dimensional structure, and provides a possible methodology to synthesize other metal oxides with special planar configurations and high performance. We believe that our primary research will inspire more valuable and profound discoveries in graphene or metal oxides.

Acknowledgements

This paper is dedicated to Prof. Daoben Zhu for his 70th birthday. The authors acknowledge the financial support from the National Natural Science Foundation of China (21077107; 20907055; 20971126; 20721061; 50725311; 51033006), the Ministry of Science and Technology of China (2011CB933700; 2011CB808400; 2009CB930400; 2007CB936602) and the Chinese Academy of Sciences.

Notes and references

1 J. R. Miller, R. Outlaw and B. Holloway, *Science*, 2010, **329**, 1637–1639.
2 M. Winter and R. J. Brodd, *Chem. Rev.*, 2004, **104**, 4245–4270.
3 Y.-G. Guo, J.-S. Hu and L.-J. Wan, *Adv. Mater.*, 2008, **20**, 2878–2887.
4 A. S. Arico, P. Bruce, B. Scrosati, J.-M. Tarascon and W. Van Schalkwijk, *Nat. Mater.*, 2005, **4**, 366–377.
5 J. Zheng, T. Jow, Q. Jia and X. Wu, *J. Electrochem. Soc.*, 1996, **143**, 1068–1070.
6 J. Zheng, P. Cygan and T. Jow, *J. Electrochem. Soc.*, 1995, **142**, 2699–2703.
7 L. Benhaddad, L. Makhloufi, B. Messaoudi, K. Rahmouni and H. Takenouti, *ACS Appl. Mater. Interfaces*, 2009, **1**, 424–432.
8 M. Toupin, T. Brousse and D. Bélanger, *Chem. Mater.*, 2002, **14**, 3946–3952.
9 H. Wang, H. S. Casalongue, Y. Liang and H. Dai, *J. Am. Chem. Soc.*, 2010, **132**, 7472–7477.
10 H. Y. Lee and J. Goodenough, *J. Solid State Chem.*, 1999, **144**, 220–223.
11 H. Chen, X. Dong, J. Shi, J. Zhao, Z. Hua, J. Gao, M. Ruan and D. Yan, *J. Mater. Chem.*, 2007, **17**, 855–860.
12 S. C. Pang, M. A. Anderson and T. W. Chapman, *J. Electrochem. Soc.*, 2000, **147**, 444–450.
13 X. Wang, W. Huang, P. Sebastian and S. Gamboa, *J. Power Sources*, 2005, **140**, 211–215.
14 V. Subramanian, H. Zhu, R. Vajtai, P. Ajayan and B. Wei, *J. Phys. Chem. B*, 2005, **109**, 20207–20214.
15 M. Xu, L. Kong, W. Zhou and H. Li, *J. Phys. Chem. C*, 2007, **111**, 19141–19147.
16 P. Yu, X. Zhang, D. Wang, L. Wang and Y. Ma, *Cryst. Growth Des.*, 2009, **9**, 528–533.
17 K. Kuratani, K. Tatsumi and N. Kuriyama, *Cryst. Growth Des.*, 2007, **7**, 1375–1377.
18 A. Zunger, S. Wagner and P. Petroff, *J. Electron. Mater.*, 1993, **22**, 3–16.
19 Z. Y. Yuan, Z. Zhang, G. Du, T. Z. Ren and B. L. Su, *Chem. Phys. Lett.*, 2003, **378**, 349–353.
20 T. Mitsuharu, A. Kazuaki and K. Hironori, *J. Electrochem. Soc.*, 1998, **145**, L49–L52.
21 C. C. Hu and T. W. Tsou, *Electrochim. Acta*, 2002, **47**, 3523–3532.
22 J. K. Chang, Y. L. Chen and W. T. Tsai, *J. Power Sources*, 2004, **135**, 344–353.
23 Y. Omomo, T. Sasaki, L. Wang and M. Watanabe, *J. Am. Chem. Soc.*, 2003, **125**, 3568–3575.
24 Z. Liu, K. Ooi, H. Kanoh, W. Tang and T. Tomida, *Langmuir*, 2000, **16**, 4154–4164.

25 Z. Liu, X. Yang, Y. Makita and K. Ooi, *Chem. Mater.*, 2002, **14**, 4800–4806.
26 E. Wortham, B. Bonnet, D. J. Jones, J. Rozière and G. R. Burns, *J. Mater. Chem.*, 2004, **14**, 121–126.
27 Z. Liu, X. Yang and K. Ooi, *J. Colloid Interface Sci.*, 2003, **265**, 115–120.
28 S. Ching, D. J. Petrovay, M. L. Jorgensen and S. L. Suib, *Inorg. Chem.*, 1997, **36**, 883–890.
29 Y. Cui, Z. H. Liu, M. Wang and K. Ooi, *Chem. Lett.*, 2006, **35**, 740–741.
30 R. Ma, Y. Bando, L. Zhang and T. Sasaki, *Adv. Mater.*, 2004, **16**, 918–922.
31 G. Zhao, L. Jiang, Y. He, J. Li, H. Dong, X. Wang and W. Hu, *Adv. Mater.*, 2011, **23**, 3959–3963.
32 G. Zhu, H. Li, L. Deng and Z. H. Liu, *Mater. Lett.*, 2010, **64**, 1763–1765.
33 S. Zhu, Z. Zhou, D. Zhang and H. Wang, *Microporous Mesoporous Mater.*, 2006, **95**, 257–264.
34 T. W. Kim, H. Yoo, I. Y. Kim, H. W. Ha, A. R. Han, J. S. Chang, J. S. Lee and S. J. Hwang, *Adv. Funct. Mater.*, 2011, **21**, 2301–2310.
35 M. Wei, Y. Konishi, H. Zhou, H. Sugihara and H. Arakawa, *Nanotechnology*, 2005, **16**, 245–249.
36 M. Polverejan, J. C. Villegas and S. L. Suib, *J. Am. Chem. Soc.*, 2004, **126**, 7774–7775.
37 A. A. Audi and P. Sherwood, *Surf. Interface Anal.*, 2002, **33**, 274–282.
38 Z. Fan, J. Yan, T. Wei, L. Zhi, G. Ning, T. Li and F. Wei, *Adv. Funct. Mater.*, 2011, **21**, 2366–2375.
39 M. Manickam, P. Singh, T. B. Issa, S. Thurgate and R. De Marco, *J. Power Sources*, 2004, **130**, 254–259.
40 M. Toupin, T. Brousse and D. Bélanger, *Chem. Mater.*, 2004, **16**, 3184–3190.
41 S. Devaraj and N. Munichandraiah, *J. Phys. Chem. C*, 2008, **112**, 4406–4417.
42 S. Chen, J. Zhu and X. Wang, *ACS Nano*, 2010, **4**, 6212–6218.
43 J. Yuan, Z. H. Liu, S. Qiao, X. Ma and N. Xu, *J. Power Sources*, 2009, **189**, 1278–1283.
44 W. S. Epling, C. H. F. Peden and J. Szanyi, *J. Phys. Chem. C*, 2008, **112**, 10952–10959.
45 L. Liu, Q. Feng, K. Yanagisawa and Y. Wang, *J. Mater. Sci. Lett.*, 2000, **19**, 2047–2050.
46 M. Wang, W. J. Lan, Y. R. Zheng, T. R. Cook, H. S. White and P. J. Stang, *J. Am. Chem. Soc.*, 2011, **133**, 10752–10755.
47 Z. Gao, J. Wang, Z. Li, W. Yang, B. Wang, M. Hou, Y. He, Q. Liu, T. Mann and P. Yang, *Chem. Mater.*, 2011, **23**, 3509–3516.